J. Fluid Mech. (1998), *vol.* 367, *pp.* 1–25. Printed in the United Kingdom

Experimental study of the stability of boundary-layer flow along a heated, inclined plate

By E. J. ZUERCHER, J. W. JACOBS AND C. F. CHEN

Department of Aerospace and Mechanical Engineering, The University of Arizona, Tucson, AZ 85721, USA

(Received 18 March 1997 and in revised form 2 February 1998)

Experiments are conducted to study the longitudinal vortices that develop in the boundary layer on the upper surface of an inclined, heated plate. An isothermal plate in water is inclined at angles ranging from 20 to 60 degrees (from the vertical) while the temperature difference is varied from 2 to 23 °C. A double-pass Schlieren system is used to visualize the vortices and particle image velocimetry (PIV) is used to measure velocities. In addition, a unique method is developed such that both the Schlieren visualization and PIV can be performed simultaneously. The wavelengths of the vortices and the critical modified Reynolds numbers ($\tilde{R}$) for the onset, merging, and breakup of the vortices are determined from Schlieren images for $Pr = 5.8$. The critical values for $\tilde{R}$ and the critical wavelengths are compared to results of previous experiments and stability analyses. The spatial growth rates of vortices are determined by using the PIV measurements to determine how the circulation in the vortices grows with distance from the leading edge. This is the first time that the growth rate of the vortices have been found using velocity measurements. These spatial growth rates are compared to the results of Iyer & Kelly (1974) and found to be in general agreement. By defining a suitable circulation threshold, the critical $\tilde{R}$ for the onset of the vortices can be found from the growth curves.

1. Introduction

It is well known that, when an inclined, heated plate is placed in a fluid, a buoyancy-induced boundary layer develops on the upper surface of the plate. This two-dimensional flow becomes unstable at a location downstream of the leading edge, and the instabilities take the form of longitudinal vortices. Downstream of their onset, the vortices undergo spanwise pairing before breaking up. The onset and development of these vortices are of interest because of their importance to applications such as chemical vapour deposition and the cooling of electronic packages. In chemical vapour deposition processes, it is advantageous to suppress the vortices so as to achieve uniform deposition. In contrast, in surface cooling, it is desirable to enhance the vortices so as to induce earlier transition to turbulence and increase heat transfer from the surface.

Several early experimental studies of this flow were performed before the presence of the vortices was detected. Rich (1953) studied heat transfer from an inclined plate using a Mach–Zehnder interferometer, but did not examine the location or the form of the instabilities that develop in the flow. On the other hand, the location of the onset of instabilities was specifically studied in the experiments of Tritton (1963), who

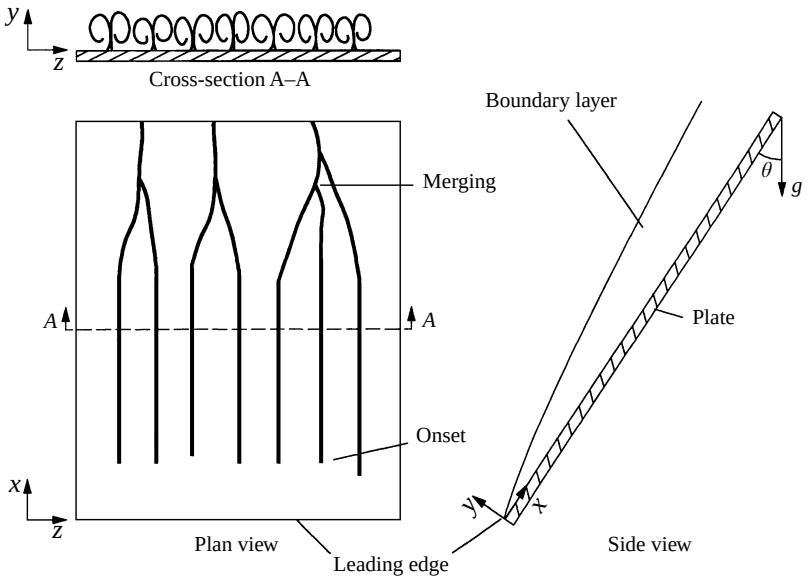

FIGURE 1. Schematic of the vortices. The dark lines in the plan view represent the outflow legs of the vortices.

measured temporal fluctuations in the velocity field, and by Lock, Gort & Pond (1967), who used a Schlieren visualization system aligned with the spanwise direction. Also, the transition to turbulence was studied by Vliet (1969) using surface temperature measurements. However, the experimental techniques of these studies did not reveal that the instability took the form of longitudinal vortices.

Longitudinal vortices were first observed in experiments by Sparrow & Husar (1969), who used an electrochemical dye technique to visualize the vortices in water, over an isothermal plate. Photographs from these experiments show an onset of vortices near the leading edge, followed by spanwise pairing of the vortices farther downstream. This is followed by what appears to be a breakup of the vortices still farther downstream. Figure 1 shows a schematic of the vortices, where the dark lines in the plan-view represent the outflow legs of the vortices. Note that, as drawn here, the spanwise wavelength of the vortices is nearly constant, until a location just upstream of the spanwise pairing. The cross-section of the vortices drawn in this figure is from a location upstream of the merging, where the vortices are parallel. (The coordinate axes defined in figure 1 are used throughout this paper.) Sparrow & Husar found that the wavelength of the vortices is nearly invariant with angle of inclination of the plate, but varies inversely with temperature difference between the plate and the ambient fluid. They also found that the onset of the vortices is moved downstream with decreasing angle of inclination from the vertical and decreasing temperature difference between the plate and the ambient fluid. Lloyd & Sparrow (1970) made more quantitative measurements using the same experimental techniques, finding a critical Rayleigh number (Ra) for the onset of instability at each angle of inclination, and comparing their results to the results of previous investigations. However, these comparisons show a large amount of scatter in the data because the earlier investigators were unaware of the presence of vortices, and it is not clear whether the critical Ra values found in previous experiments indicated the onset or the breakup of the vortices. Lloyd & Sparrow also found that the vortices did not appear for angles from vertical of less than

14 degrees, and that the vortices coexisted with Tollmien–Schlichting wave instabilities between 14 and 17 degrees. Lloyd (1974) studied the wavelength of the longitudinal vortices over an isothermal plate in water, using the same technique as that of Sparrow & Husar. He obtained a relation between the temperature differences and the spanwise wavelength, and confirmed that the wavelength is nearly invariant with angle of inclination.

One other experimental investigation of the vortices on an isothermal plate was performed by Cheng & Kim (1988), who used smoke to visualize the vortices in air for low angles of inclination from horizontal. Wavelengths and critical Grashof numbers for the onset of vortices were found and agree qualitatively with the results of the previous studies. However, the angles studied were closer to horizontal than those investigated in the earlier experiments, and so quantitative comparisons with the results of Lloyd & Sparrow (1970) are difficult.

In addition to the studies on an isothermal plate, one experimental investigation of the onset and wavelength of the vortices on a constant heat flux plate has been performed. Shaukatullah & Gebhart (1978) measured local temperatures and velocities using thermocouples and constant temperature hot-film anemometers. A spanwise variation in fluid velocities was observed, indicating the presence of longitudinal vortices, and the onset and wavelength of these vortices were determined. In addition, growth rates were calculated from temperature measurements. The effects of the angle of inclination and temperature difference on the onset locations and wavelengths of the vortices agree qualitatively with those of earlier investigations, but quantitative comparisons are not appropriate because of the different boundary conditions at the plate.

The onset of the vortices has been studied analytically, as well as experimentally, using linear stability theory. Haaland & Sparrow (1973) performed a temporal linear stability analysis in which some non-parallel flow effects were taken into account, and numerical integration was performed. They determined that the parallel flow assumption does not lead to the correct behaviour at the outer edge of the boundary layer, and a modified parallel flow assumption allowing for flow normal to the plate was used instead. A modified Reynolds number ($\tilde{R}$) was introduced in place of the Rayleigh number, which has the advantage of providing critical values that are independent of the angle of inclination of the plate. Neutral stability curves were found. As was observed experimentally, the onset of instabilities is moved downstream with decreasing angle from the vertical; however, the predicted onset occurs much farther upstream than was observed experimentally by Lloyd & Sparrow (1970). Iyer & Kelly (1974) postulated that these experiments were not sensitive enough to detect the first instabilities predicted by theoretical analyses. Thus, using a spatial linear stability analysis with the parallel flow assumption, Iyer & Kelly examined the formation and growth of both wave instabilities and longitudinal vortices, and attempted to find a correlation between experimental and theoretical results by finding the total amplification between the earliest disturbances and the observed disturbances. Chen & Tzuoo (1982) included the gravity component, which acts perpendicular to the plate in their temporal stability analysis. However, their results show that the inclusion of the gravity component in the analysis does not change the predicted critical $\tilde{R}$ significantly, and the onset of the vortices was again predicted to occur far upstream of where it was observed experimentally by Lloyd & Sparrow.

While most stability analyses deal with the onset of the vortices, another important transition in this flow is the pairing and breakup of the vortices. The photographs of Sparrow & Husar (1969) reveal that the longitudinal vortices merge and finally break

up at a downstream location; however, this transition has not been specifically studied in subsequent experiments. Chen *et al.* (1991) performed a temporal stability analysis that studied the locations of the onset and the merging and annihilation of the vortices, formulating the problem in the same manner as Haaland & Sparrow (1973). As in the case of onset, the merging and breakup of the vortices observed in the photographs of Sparrow & Husar occur much farther downstream than predicted by the stability analysis.

The present study attempts to re-examine the formation and growth of the vortices experimentally. It differs from previous experiments in that it includes both visualization and velocity measurements of the flow, which allows the flow visualization to be correlated to the velocity field. In addition to investigating the streamwise location of onset of the vortices, the present study also examines the locations of the merging and breakup of the vortices so that for the first time comparisons with the stability analysis of Chen *et al.* (1991) can be made. Finally, fluid velocity measurements are used to determine spatial instability growth rates by measuring the circulation in the vortices at successive streamwise locations. These results are compared with the calculations of Iyer & Kelly (1974).

2. Experimental apparatus

The experimental apparatus, shown in figure 2, consists of an isothermally heated plate set in a water tank, which is mounted on a beam that can be inclined up to 60 degrees from the horizontal. The plate is mirrored high-transmission float glass with dimensions 0.3175 cm thick $\times$ 11.43 cm wide $\times$ 35.56 cm long. The surface temperature of the plate is measured by eight thermocouples set in holes in the back of the plate to within 0.09 cm of the surface. Because of the relatively low thermal conductivity of glass, the temperature difference between the plate and the ambient varies by approximately 10% over the plate. Spanwise and streamwise locations are marked on the glass using waterproof ink. The glass has been made into a second surface mirror for the Schlieren experiments by coating the back of the glass with black paint. The glass is fixed with type Z9 silicone heat sink compound to a brass plate with dimensions 1.27 cm thick $\times$ 11.43 cm wide $\times$ 30.48 cm long, and the joint between the brass plate and glass plate is sealed with a waterproof fibreglass resin. The brass plate is kept at a constant temperature by an antifreeze–water mixture, which is circulated through slots milled in it. The heating mixture is kept at the desired temperature by a Lauda RK20 heating bath with an accuracy of 0.01 °C. Measurements show that the temperature of the fluid entering and leaving the heated brass plate varies by less than 0.1 °C. Edge effects at the longitudinal edges of the plate are minimized by 2.6 cm high Plexiglas fences. Fences such as these were also used by Sparrow & Husar (1969).

The plate is mounted near the back of a Plexiglas tank with dimensions 56 cm $\times$ 28 cm $\times$ 46 cm. The side of the tank opposite the upper surface of the plate is high-transmission float glass, and the Schlieren and PIV images are obtained through this side of the tank. The tank is secured to a 15 cm $\times$ 30 cm $\times$ 200 cm wood beam, which is hinged so that it can be inclined at any angle from 0 to 60 degrees from the horizontal. The hinge is placed in a location such that a cable at the end of the beam opposite the tank is always in tension. Thus, the angle of inclination of the apparatus can be adjusted by a winch attached to this cable.

A double-pass Schlieren system is also mounted on the beam. Two spherical mirrors mounted at the end of the beam opposite the tank direct light from a point light source toward the plate. (Two mirrors were used rather than one for added field of view.) The

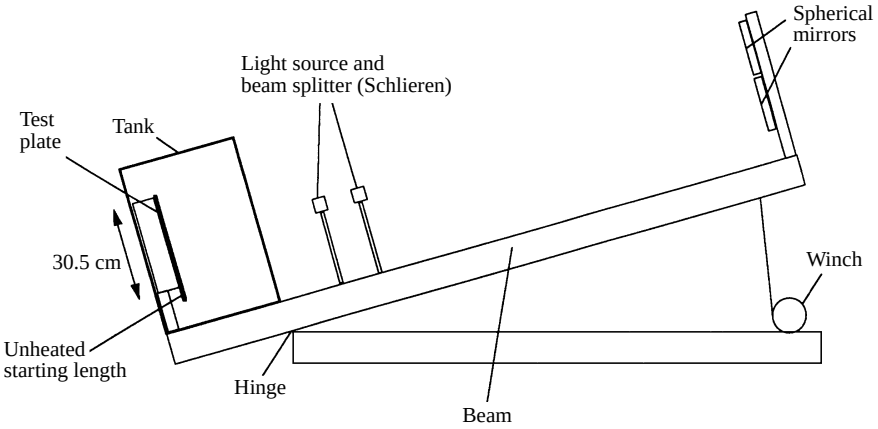

FIGURE 2. Side view of the inclined beam with the tank.

light reflected from the plate is then directed into a Cohu Model 4915 CCD camera by a beam splitter. A knife edge is placed between the beam splitter and camera. Because both the water tank and Schlieren system are mounted on the inclined beam, the Schlieren view is normal to the tank and plate for any plate inclination, and diffraction of light between water and air is never a concern.

The PIV system was developed at the University of Arizona in the Hydrodynamics Laboratory, using the basic techniques for particle image velocimetry described by Adrian (1991) and Willert & Gharib (1991). Images acquired by another Cohu Model 4915 CCD camera are digitized by a PDI IMAXX Video Capture Board and analysed on a Power Macintosh computer. The velocities in the flow field are low enough that no laser or camera shuttering is necessary. Interrogation regions in successive images are cross-correlated to achieve fluid displacements, and the displacements are divided by the time-interval between the images to achieve velocity vectors. The full captured image resolution is 768×486 pixels, while the interrogation region size for most calculations is 64×64 pixels. The particles used to seed the flow are polycrystalline, with a diameter of 30 μm and a specific gravity close to that of water. A 2 W argon ion laser provides the light to illuminate the flow, and a series of three optical lenses is used to focus the laser beam into the appropriate sheet. The laser sheet is set perpendicular to the plate when used for measuring the growth of circulation in the longitudinal vortices. Because of the large flow velocity along the plate, the laser sheet was expanded to 1 cm thick in order to keep enough PIV particles in the illuminated volume to obtain successive frames for accurate measurements. The accuracy of the PIV system was measured by traversing a camera relative to a printed field of white dots. These tests indicated that the velocity measurements have a maximum error of 5%. A more detailed discussion of the PIV system and experimental apparatus can be found in Zuercher (1996).

Initially, the ambient fluid is uniformly at rest. When heat is applied to the plate, a steady state plate temperature is reached within approximately 4 min. The vortices are also present and uniform at this time. As the experiment progresses, a vertical temperature gradient develops in the ambient fluid that is caused by the build-up of the heated water exiting the trailing edge of the plate. The experiment is halted when this temperature gradient exceeds 0.040 °C cm^{-1}, which allows for at least 15 min of run time. Vertical temperature gradients of less than this limit do not appear to affect the characteristics of the flow. Lloyd & Sparrow (1970) cite a limit of 0.045 °C cm^{-1}.

3. Leading-edge considerations

Preliminary experiments showed that the flow on the plate is very sensitive to boundary conditions, particularly to conditions at the leading edge. Thus, the suitability of several different leading-edge set-ups was investigated. The ideal leading edge for the experiment would be sharp and isothermal. However, this leading-edge condition is very difficult to implement in practice, and particularly in the present experiments as the glass plate is fixed to a thick brass plate. Any portion of the glass plate not in contact with the brass plate would no longer be isothermal. A survey of the literature shows that other investigators have encountered similar problems and that there has been no consensus on the best leading-edge set-up. An unheated ledge perpendicular to the plate at the leading edge was used by Vliet (1969), an unheated starting length was used by Shaukatullah & Gebhart (1978), and a leading edge with a radius was used by Lock *et al.* (1967). The major source of experimental data on the subject, Lloyd & Sparrow (1970), does not indicate what leading-edge conditions were used. The three leading-edge set-ups tested in the present experiments are shown in figure 3. It was found that when the leading edge was untreated (figure 3*a*), heated fluid from the front edge of the heated brass plate was convected around the lip of the leading edge and contributed to the boundary-layer flow on the plate. This leading-edge condition is unacceptable because the ideal leading edge should only provide heating on the upper surface of the plate to drive the flow. The second and third leading-edge configurations for which experiments were conducted were an unheated starting length made by extending the mirrored glass plate beyond the edge of the heated brass plate and an unheated ledge perpendicular to the glass plate at the leading edge (figures 3(*b*) and 3(*c*), respectively). While both of these leading edges yielded similar results for the location of the transition point in the flow and the spanwise wavelength of the vortices, the unheated starting length was used for the data presented in this study because the PIV measurements described below indicate that it leads to a flow that is in satisfactory agreement with a theoretical solution.

The performance of the unheated starting length was tested by finding the velocity profiles in the (x, y)-plane of the boundary layer on a vertical, isothermal, heated plate. The velocity boundary layer on such a plate has been solved analytically using a similarity solution and confirmed by experiments (summarized in Ede (1967)). The theoretical boundary-layer solution should be valid from approximately 1 to 15 cm from the leading edge under the present experimental conditions (Gebhart *et al.* 1988). Upstream of 1 cm, the boundary-layer-flow approximation does not apply, while downstream of 15 cm the flow becomes unsteady. The solution for the base flow on the inclined plate used by Chen *et al.* (1991) is identical to that of the vertical plate, except for a correction in the gravity force for the angle of inclination. The velocity profiles can be normalized into a single profile using the similarity variables suggested by theory:

$$\eta = \frac{y\kappa}{x^{1/4}}, \tag{3.1}$$

and

$$F(\eta) = \frac{\psi}{4\nu\kappa x^{3/4}}. \tag{3.2}$$

Here,

$$\kappa x^{3/4} = \left[\frac{\beta g(\Delta T)\cos\theta x^3}{4\nu^2}\right]^{1/4} = \left[\frac{Gr_x\cos\theta}{4}\right]^{1/4}, \tag{3.3}$$

$$\kappa = \left[\frac{\beta g\cos\theta(\Delta T)}{4\nu^2}\right]^{1/4}, \tag{3.4}$$

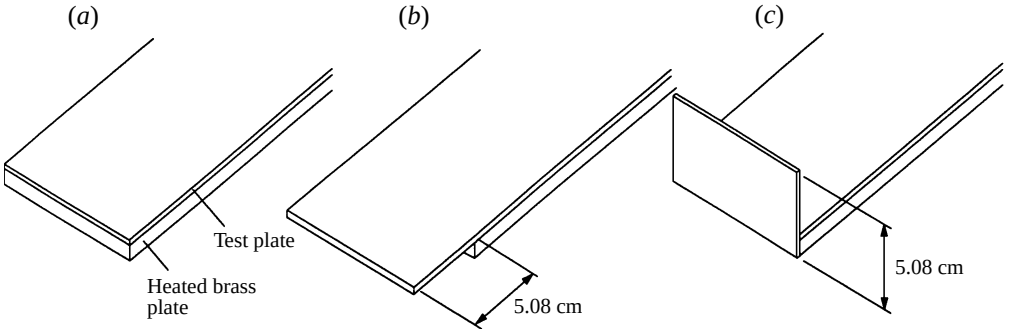

FIGURE 3. The three leading edges: (*a*) untreated, (*b*) unheated starting length, and (*c*) unheated ledge.

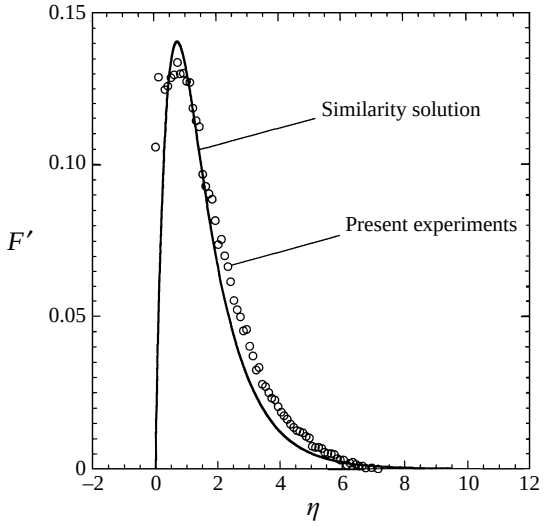

FIGURE 4. Comparison of velocity profiles from present experiments and similarity solution, both for a vertical plate. η is the scaled distance normal to the plate and F' is the scaled velocity.

ψ is the stream function, x is the distance from the start of the heated region of the plate, β is the thermal coefficient of expansion, g is gravity, ν is the kinematic viscosity, ΔT is the temperature difference between the plate and the ambient fluid, θ is the angle the plate makes with the vertical, and Gr_x is the Grashof number defined in terms of the distance from the leading edge. Figure 4 compares the similarity solution to data obtained with a vertical plate from five scaled profiles obtained between 5 and 7 cm from the start of the heated region of the plate. This plot shows that the measured velocity distribution agrees well with the theoretical flow. Since the flow is generated by the imposed temperature difference, it is expected that the temperature distribution also agrees with the theoretical prediction. Shaukatullah & Gebhart (1978) showed that such good agreements do exist for both the velocity and temperature profiles along a plate inclined at 19° from the vertical with a constant heat flux boundary. Kierkus (1968) showed that by using the reduced gravity $g\cos\theta$, such agreements can be obtained for plate inclination angles up to $\theta = 45$ degrees. In the present paper, it is shown that data can be correlated by using the reduced gravity for a range of θ from 20 to 60 degrees.

In addition, velocity measurements obtained farther upstream show that for $\Delta T =$

10 °C the flow begins approximately 1 cm upstream of the start of the heated portion of the plate. A fin analysis shows that there is some conduction of heat from the heated portion of the plate into the unheated starting length and, for $\Delta T = 10$ °C, the temperature difference between the plate and the ambient fluid falls to 10% of its maximum value approximately 7–10 mm from the start of the heated regions. Since there is essentially no flow upstream of this location, the length of the unheated starting length is not important as long as it extends beyond this incidentally heated region. This test shows that the boundary-layer flow on the plate with an unheated starting length is in good agreement with the boundary-layer flow found analytically using an ideal leading edge. Thus, the unheated starting length was used throughout the present experiments.

4. Schlieren results

The Schlieren data were used to confirm qualitatively the results of previous experiments and analyses, and to observe the streamwise locations where the vortices merge and break up for comparison with the analysis of Chen *et al.* (1991). For this set of experiments, the vortices were allowed to develop naturally without forcing. Figure 5 shows three typical plan views of the flow as seen using the Schlieren apparatus. Each of the two visible regions corresponds to a spherical mirror. The dark space between the two visible regions is space between the mirrors, which unfortunately could not be eliminated. The leading edge is at the right-hand side of the images, and the flow moves downstream to the left-side of the images. The vortices appear as dark streaks adjacent to light streaks. Using velocity measurements obtained from simultaneous PIV, it was determined that the outflow legs of the vortices are located where the dark streaks abut the light streaks (see discussion in § 5). The dark and light streaks are caused by spanwise temperature gradients in the flow, which arise where the hot outflow legs of the vortices are adjacent to the cooler inflow.

4.1. *Onset and breakup of the vortices*

Several transition points can be identified from the Schlieren images. The first of these is the onset of the vortices (point (*i*) in figure 5*a*). This point is defined as the streamwise location at which one or more vortices first become visible in the Schlieren images. For some vortices, a second transition occurs where the vortices begin to move in the spanwise direction (point (*ii*) in figure 5*a*). Upstream of this location the vortices are nearly parallel and stationary, even when time-lapse video is used to view the experiment twelve times faster than real time. Downstream of this location, these vortices are no longer uniformly parallel. When viewed using time-lapse video, these vortices move in the spanwise direction, appearing somewhat like tree tops waving in the wind. A third transition point occurs where the vortices merge (point (*iii*) in figure 5*a*). Usually, two vortex pairs merge into one pair, although sometimes three vortex pairs appear to merge into one pair. Finally, a fourth transition point can be identified where the vortices begin to break up. Downstream of this location, vortices may still be observed; however, they periodically break down into random structures. Also, random structures are present in the relatively large spaces between adjacent vortices. The merging and breakup of the vortices in these experiments occur close to each other spatially and are usually indistinguishable from each other; therefore, the two points were combined as one transition point and referred to as the point of breakup. One weakness in this type of measurement is that the determination of transition points is somewhat subjective. The locations of the transitions vary slightly from vortex to

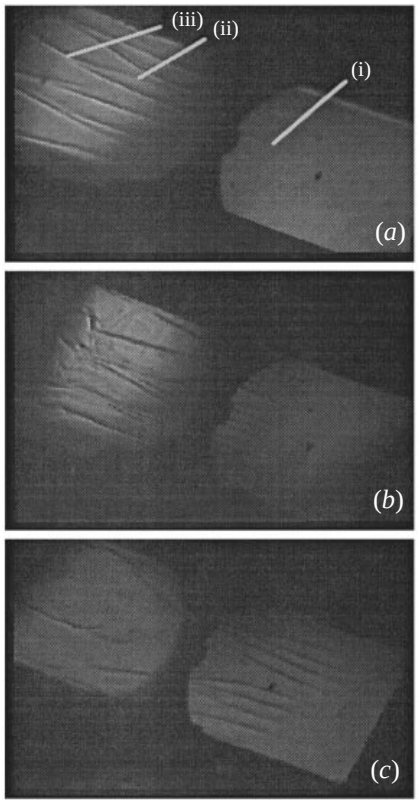

FIGURE 5. Schlieren plan view of the flow with $Pr = 5.8$ for three different sets of parameters. Flow conditions are: (*a*) $\theta = 40$ degrees, $\Delta T = 5$ °C (with transition points: (*i*) onset, (*ii*) unsteady, and (*iii*) merging/breakup); (*b*) $\theta = 40$ degrees, $\Delta T = 12.5$ °C; and (*c*) $\theta = 60$ degrees, $\Delta T = 5$ °C.

vortex and are not always clearly defined. This problem is also evident in the photographs of Sparrow & Husar (1969) and was reported by Lloyd & Sparrow (1970).

Three typical images are shown in figure 5, illustrating the flow for three different conditions, all with $Pr = 5.8$. Figure 5(*a*) shows the flow for $\theta = 40$ degrees and $\Delta T = 5$ °C. Here the vortices have a wavelength of approximately 12.5 mm and appear to begin 10 cm from the start of the heated region of the plate. They merge and break up 25 cm from the start of the heated region. Figure 5(*b*) shows the flow for $\theta = 40$ degrees and $\Delta T = 12.5$ °C. Here the vortices have a wavelength of approximately 8.5 mm, begin 8 cm from the start of the heated region of the plate, and merge 21 cm from the start of the heated region. Figure 5(*c*) shows the flow for $\theta = 60$ degrees and $\Delta T = 5$ °C. The wavelength of the vortices is approximately 11.5 mm, and the vortices begin 4 cm from the start of the heated region. The vortices merge and break up at 9.5 cm from the start of the heated region. Beyond the merging point, two vortices survive for a short distance; the rest of the image appears to be random motion. As is evident from the comparison of these three images the onset and breakup of the vortices are moved upstream with increasing temperature difference and angle of inclination.

Stability theory indicates (Haaland & Sparrow 1973) that for each value of Pr the onset and breakup of the vortices can be described by a critical modified Reynolds number, $\tilde{R}$:

$$\tilde{R} = 4\kappa x^{3/4} \tan\theta = 4 \left(\frac{Gr_x \cos\theta}{4} \right)^{1/4} \tan\theta. \tag{4.1}$$

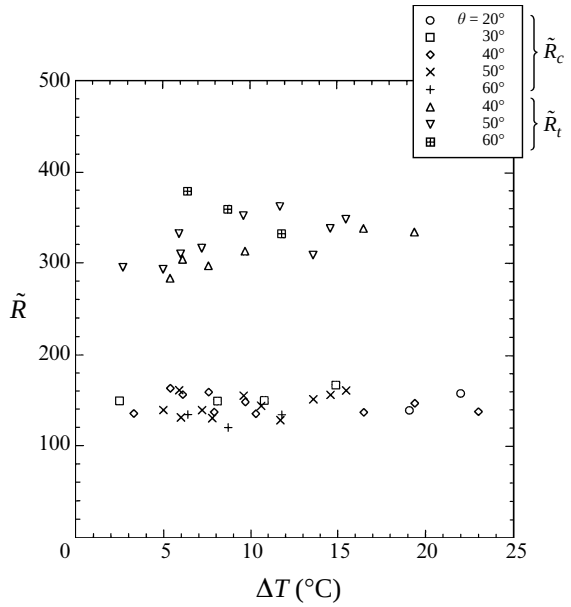

FIGURE 6. $\tilde{R}_c$ and $\tilde{R}_t$ for $20° \leqslant \theta \leqslant 60°$ and $2\ °C \leqslant \Delta T \leqslant 23\ °C$.

Since $(Gr_x \cos\theta)^{1/2}$ is the equivalent Reynolds number of a natural convection flow along an inclined, heated plate, the modified Reynolds number, $\tilde{R}$, is proportional to the square root of the equivalent Reynolds number with an angular modification. The validity of using a critical $\tilde{R}$ to describe the locations of the transitions in the flow was tested in the present study by performing experiments with $Pr = 5.8$ and finding the critical values of $\tilde{R}$ for the onset and breakup of the vortices. A total of 32 experiments was performed, with θ varying from 20 to 60 degrees, by increments of 10 degrees, and ΔT varying from 2 °C to 23 °C. The variations in Pr were limited to 10% between experiments, and Pr for most of the experiments was within 5% of Pr for all other experiments. Figure 6 shows the critical values of $\tilde{R}$ for the various values of θ and ΔT. While there is some scatter in the data, there is no clear trend. On average, the vortices were found to appear at $\tilde{R}_c = 145$, with a 95% confidence interval of ± 5, and to break up at $\tilde{R}_t = 330$, with a 95% confidence interval of ± 20. These uncertainties are mainly due to the uncertainty in locating the transition points.

The good collapse of the data using critical values of $\tilde{R}$ for the onset and breakup of the vortices indicates that stability theory is correct in predicting that the locations of these transitions are described by $\tilde{R}$; however, the quantitative values for critical values of $\tilde{R}$ found experimentally do not match those predicted by stability theory. The temporal stability analysis of Chen *et al.* (1991) finds $\tilde{R}_c = 24.26$ and $\tilde{R}_t = 49.95$ for $Pr = 5.5$. While these values for $\tilde{R}_c$ and $\tilde{R}_t$ differ widely from those found experimentally, the values of the ratio $\tilde{R}_t/\tilde{R}_c$ are quite close ($\tilde{R}_t/\tilde{R}_c = 2.1$ for Chen *et al.*, while $\tilde{R}_t/\tilde{R}_c = 2.3$ for the present experiments). A value of $\tilde{R}_c = 95$ can be deduced from the experimental data of Lloyd & Sparrow (1970). While Lloyd & Sparrow did not tabulate data on the location of the breakup of the vortices, a value of $\tilde{R}_t = 188$ can be deduced from the photograph in figure 1 of Sparrow & Husar (1969). (The experimental apparatus of Sparrow & Husar is identical to the apparatus of Lloyd & Sparrow.) For comparison purposes, the distances from the leading edge to the onset of the vortices from the stability analysis of Chen *et al.*, the experiments of Lloyd &

Sparrow, and the present experiments for $\theta = 30$ degrees, $\Delta T = 10$ °C, and $Pr = 5.8$ are 1.1, 8 and 13 cm, respectively.

There are several possible explanations for the disparity between the results of experiments and stability analyses for the locations of the transition points. First, the sensitivity of the visualization systems of both the present experiments and the experiments of Lloyd & Sparrow (1970) are limited. Linear stability analyses define the most upstream location at which an infinitesimal perturbation begins to grow as the onset of instability. However, this perturbation must grow to a certain magnitude before it is detectable by measurement devices. Therefore, the onset of instability may occur far upstream of where it is first detected experimentally. It is difficult to quantify the sensitivity of the Schlieren system. Furthermore, the sensitivity of the visualization system used by Lloyd & Sparrow is unknown. On the other hand, there is no question of the effect of the sensitivity of the method of visualization on the determination of the locations of the merging and breakup of the vortices, as the vortices are well-developed at the location at which they merge and are plainly visible. Therefore, the sensitivity of the experimental apparatus does not explain the disparity between Chen *et al.*'s predicted location of the breakup of the vortices and the experimentally observed location of the breakup.

Secondly, disparity between the results of the present experiments and those of Lloyd & Sparrow (1970) could be caused by differences in each researcher's interpretation of experimental images. In the present experiments the onset of vortices was defined as the streamwise location at which the vortices first become visible; however, when the photographs of Sparrow & Husar (1969) are examined in conjunction with the data of Lloyd & Sparrow, it appears that the onset of vortices was not defined in this way by Lloyd & Sparrow. When the photographs of Sparrow & Husar (1970) are subjected to the same onset criteria as are used in the present experiments, the vortices appear to start at the leading edge rather than where reported by Lloyd & Sparrow.

Finally, the conditions at the leading edge influence the behaviour of the flow. The importance of leading-edge conditions was confirmed in the present experiments when the untreated leading edge was used and the vortices were observed to arise directly at the leading edge of the plate, so that $\tilde{R}_c = 0$. The location of the breakup of the vortices was also observed to move upstream, occurring at $\tilde{R}_t = 214$. The leading-edge conditions used by Lloyd & Sparrow (1970) are unknown, but their results appear similar to the results obtained in the present experiments with the untreated leading edge. For example, the onset of the vortices in the first photograph in figure 1 of Sparrow & Husar (1969) appears to occur at $\tilde{R}_c = 0$, which is identical to the results obtained in the present experiments with the untreated leading edge. In addition, the breakup of the vortices appears to occur at approximately $\tilde{R}_t = 188$ in this photograph, which is within 13 % of the value found in the present experiments with the untreated leading edge. Because of these similarities, and because Lloyd & Sparrow make no mention of their leading-edge conditions, it is probable that an untreated leading edge was used. In the present experiments, the unheated starting length was found to lead to flow in good agreement with the theoretical boundary-layer base flow. Therefore, the problem of leading-edge conditions is more likely to explain the disparity in the results of the present experiments and those of Lloyd & Sparrow than the disparity with the stability analysis of Chen *et al.* (1991).

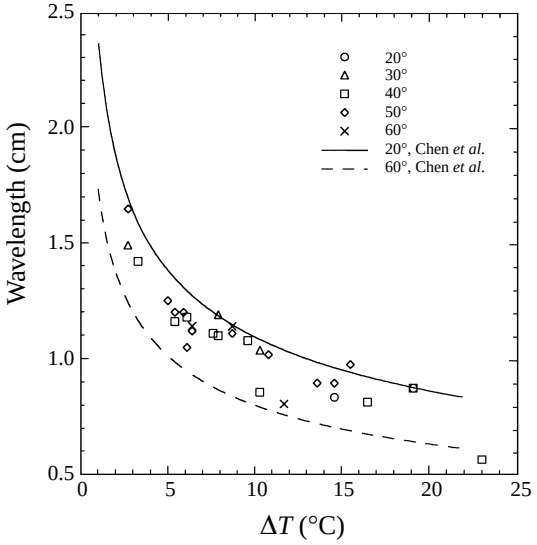

FIGURE 7. Wavelength *vs.* ΔT. The experimentally determined $\tilde{R}_e$ is used to dimensionalize the results of Chen *et al.* (1991).

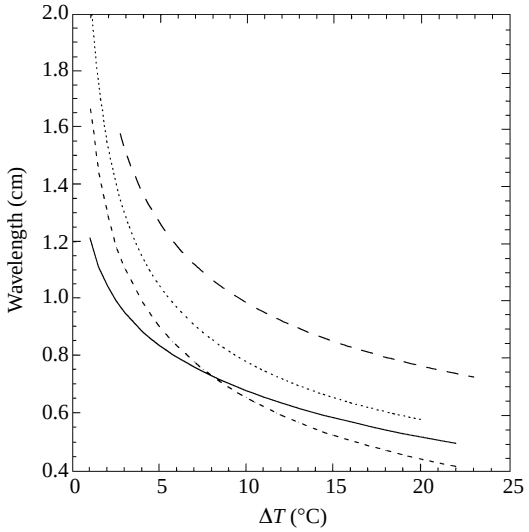

FIGURE 8. Wavelength *vs.* ΔT compared for two leading-edge conditions (— — —, unheated starting length; ···, untreated leading edge), ———, the experiments of Lloyd (1974), and – – –, the stability analysis of Chen *et al.* (1991), angle = 20 degrees.

4.2. *Wavelength of the vortices*

The spanwise wavelength of the vortices is another quantity that the Schlieren visualization was useful in determining. Extensive wavelength data have been gathered by Lloyd (1974), so the wavelength data of the present experiments are not meant to be complete but are only to be used for comparison with the results of the previous experiment and with stability theory. The wavelength of the vortices was taken to be the mean spanwise distance between the dark streaks visible on the Schlieren set-up, which are known from the PIV measurements to be the outflow legs of the vortices. Figure 7 shows the wavelength of the vortice plotted versus the temperature difference

between the plate and ambient fluid, with $Pr = 5.8$ for all data. The wavelengths at each angle of inclination are indicated with different markers. In addition, these wavelengths are compared with the theoretical critical wavenumber of Chen *et al.* (1991), which have been made dimensional. Note that the analysis of Chen *et al.* defines a dimensionless critical wavenumber, α_c, as

$$\alpha_c = \frac{2\pi}{\lambda_c}\left(\frac{\tilde{R}_c}{4}\right)^{1/3}(\tan\theta)^{-1/3}\kappa^{-4/3}, \tag{4.2}$$

which uses the streamwise distance from the leading edge to the onset of the vortices to scale the dimensional critical wavelength, λ_c. However, the distance to onset found experimentally is much greater than the distance found from the stability analysis, as was previously discussed. In figure 7 the experimentally determined distance to onset is used to dimensionalize Chen *et al.*'s wavenumber data, with good results, as nearly all experimentally determined wavelengths fall within the limits predicted by the stability analysis. The average critical wavenumber, α_c, found experimentally was 1.03, which compares to $\alpha_c = 1.27$ from the stability analysis of Chen *et al.* The stability analysis finds that the wavelength of the vortices varies slightly with angle of inclination, growing longer as the angle from the vertical is decreased. However, the amount of wavelength data obtained in the present experiments is not sufficient to indicate this.

In addition to the data obtained with the unheated starting length edge, wavelength measurements were also acquired with the untreated leading edge. While this leading-edge condition leads to poor flow characteristics, it was thought that it might be useful in measuring wavelengths. Because the untreated leading edge fixes the onset of the vortices near the leading edge and makes them more uniform, wavelength measurements are simplified. However, it was found that the wavelengths that arose with an untreated leading edge were different from those found using the unheated starting length. Least-square fits of the wavelength data for the untreated leading edge and unheated starting length are compared in figure 8, which shows that the wavelengths of the vortices that arose with the untreated leading edge are shorter than those that arose with the unheated starting length. It appears that the distance from the leading edge to the onset of the vortices has an effect on the wavelength of the vortices, in that a shorter distance to onset leads to shorter wavelengths. This is supported by comparisons with the experimental data of Lloyd (1974) and the theoretical data of Chen *et al.* (1991) in figure 8, where the non-dimensional data of Chen *et al.* is scaled using the analytically obtained distance from the leading edge to the vortices. Both Lloyd's experimental data and Chen *et al.*'s theoretical data show the vortices starting farther upstream and with shorter wavelengths than the data of the present experiments. (Lloyd does not actually specify any critical distances for the onset of vortices, but used the experimental set-up of Lloyd & Sparrow (1970), who found a shorter distance to the onset of the vortices than in the present experiments.) This relationship is also implied by equation (4.2) which defines the critical wavenumber, α_c, in terms of distance from the leading edge, and explains why the widely differing values of $\tilde{R}_c$ and λ_c determined experimentally and theoretically lead to similar values for α_c.

5. PIV results

The PIV system was used to obtain velocity fields of the developing vortices. Because the experimental set-up allowed the simultaneous acquisition of Schlieren and velocity data, it was possible to correlate velocity fields with the Schlieren images. In addition,

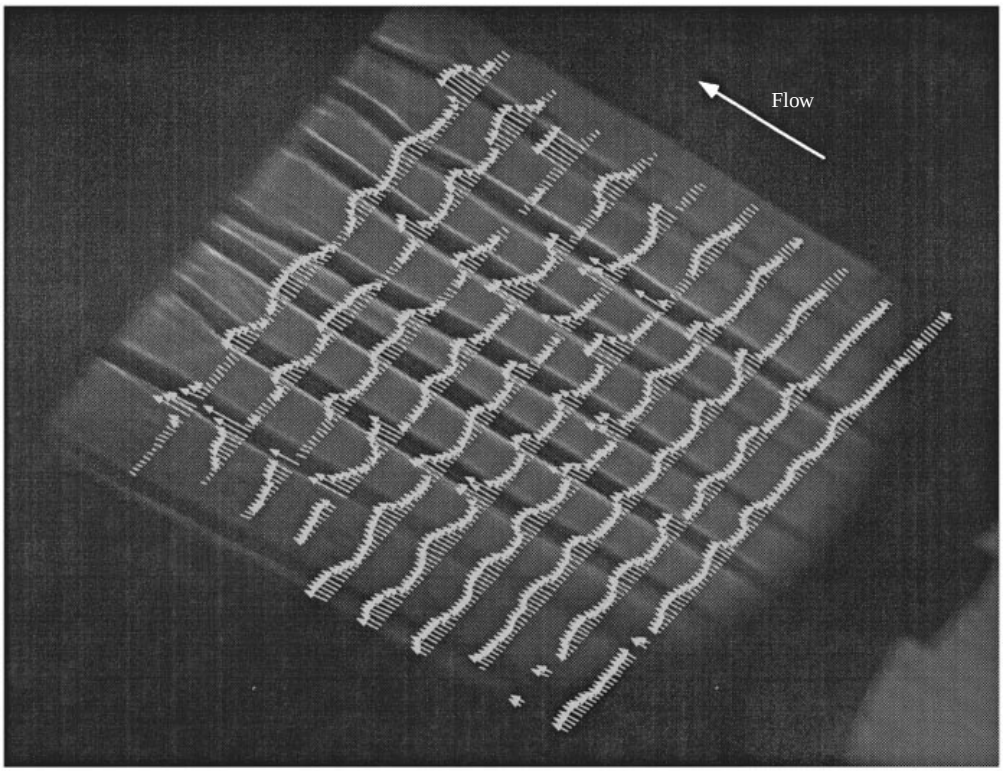

FIGURE 9. Plan view of the velocity field superimposed on a shadowgraph image.

the velocity fields were used to find the growth rates of the vortices and to quantitatively define an onset location for the vortices.

5.1. *Correlation of the Schlieren images to the velocity field*

The Schlieren flow visualization was correlated to the velocity field for two different laser sheet orientations. Figure 9 shows the first orientation, a plan view of the flow. Here, the velocity field from a plane 2 mm above and parallel to the plate is superimposed on a shadowgraph image of the vortices. The streamwise locations of the velocity vectors range from 17 to 24 cm from the start of the heated region of the plate, with flow conditions of $Pr = 5.8$, $\theta = 30°$, and $\Delta T = 8.6$ °C. The time interval between the shadowgraph image and the images acquired for the PIV measurements is 1 s, and the maximum velocity in this plane is 32.9 mm s^{-1}. The dark streaks on the shadowgraph image are the hottest portions of the flow and correspond to where the dark and light streaks in Schlieren image abut. Thus, this image reveals that the hottest portions of the flow have the highest streamwise velocity.

The second orientation of the laser sheet was created by directing the laser sheet in the (y, z)-plane, perpendicular to the plate and aligned with the spanwise direction, which yields a cross-section of the vortices. A typical velocity field and its corresponding constant vorticity contours are shown in figure 10. The conditions for this flow are $Pr = 5.8$, $\theta = 60°$, and $\Delta T = 10$ °C. This (y, z)-plane cuts through the flow 7 cm from the start of the heated region of the plate, which is the most downstream location at which the vortices are all steady and uniform. Two and one-half vortex-pairs are visible in this view, and the wavelength is 1 cm. As might be expected, the direction of rotation of the circulation regions alternate as one moves across the plate in the spanwise

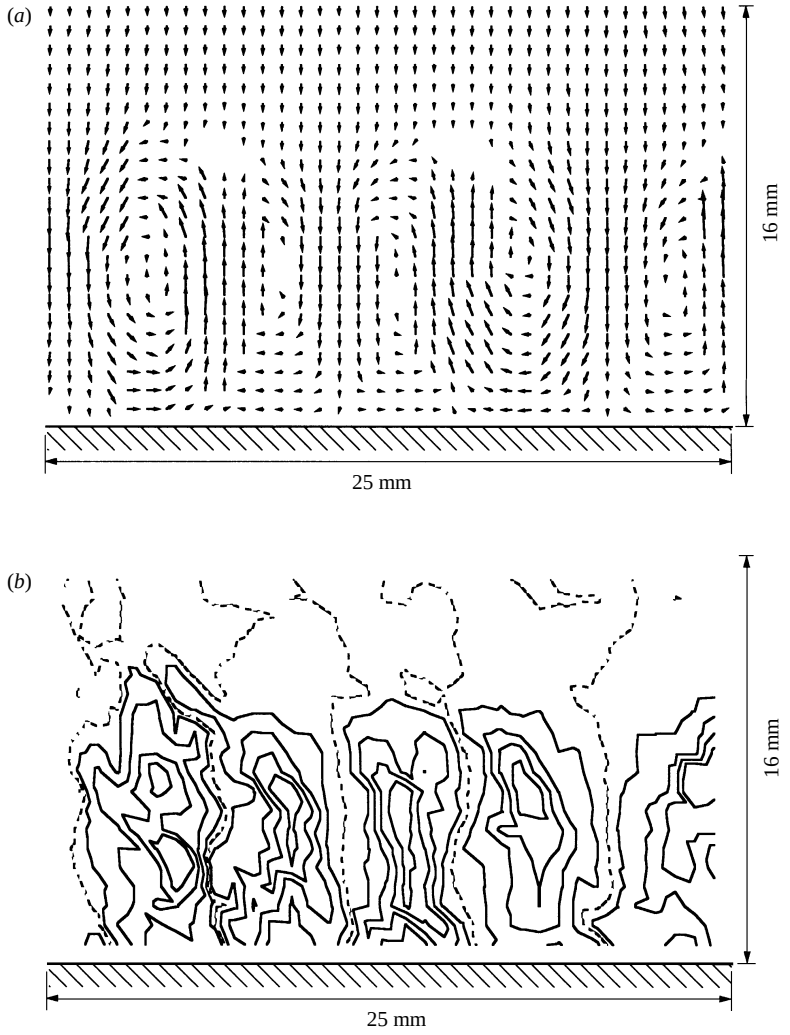

FIGURE 10. (*a*) Typical velocity field in the (y, z)-plane; (*b*) corresponding contours of constant vorticity.

direction. The several regions in figure 10(*a*) where there are no vectors, are portions of the flow where there is very low velocity. Above the vortices, there is a nearly uniform inflow toward the plate owing to entrainment. The vorticity field shown in figure 10(*b*) was found by centred-differencing the velocity field in figure 10(*a*). The dashed lines are lines of zero vorticity. It is expected that the vorticity should go to zero above the vortices; however, in the experimental data, some very low values of vorticity persist above the vortices.

A velocity field such as that of figure 10 was correlated with the Schlieren images. This process was performed by acquiring Schlieren and PIV images simultaneously and comparing the velocity field to the Schlieren image. The plan view shown in figure 9 indicates that the hottest regions of the flow also have the greatest streamwise velocity; however, it does not reveal which region of the vortices contains the hottest fluid. It might be expected that the fluid in the outflow legs of the vortices is the hottest, as it has just been heated by the plate. However, the isotherms plotted in figure 6(*b*) of Chen

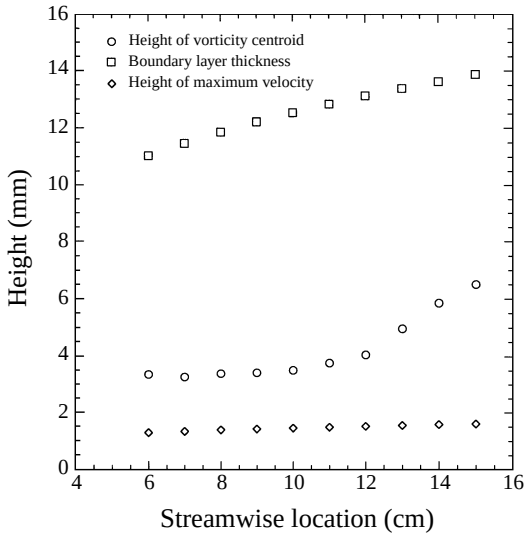

FIGURE 11. Variation of the height of the centroid of the vorticity in the vortices, the maximum velocity in the boundary-layer base flow, and the outer edge of the velocity boundary-layer base flow with streamwise distance from the start of the heated region of the plate. Note that downstream of 12 cm the vortices grow faster than the boundary-layer base flow.

et al. (1991) call this into question, as the isotherms plotted are concentric circles centred at the core of the vortices. This contradiction was resolved in the present experiments when the velocity field in the (y, z)-plane was correlated with a Schlieren image, which revealed that the outflow legs of the vortices do indeed correspond with the hottest portions of the flow. This correlation is in agreement with figure 5 of Moutsoglou, Chen & Cheng (1981), which plots streamlines and isotherms for convective vortices on a horizontal plate, and with the measurements of Shaukatullah & Gebhart (1978) for flow within the boundary layer.

An interesting result found from the PIV data was that the height of the vortices grows faster than the thickness of the boundary-layer base flow. Figure 11 compares the height of the centroid of the vorticity in the vortices for a typical experiment with the height of the maximum velocity in the theoretical boundary-layer base flow and the outer edge of the theoretical boundary layer. The conditions for this flow are $Pr = 5.8$, $\theta = 40°$, and $\Delta T = 10\ °C$. Downstream of 12 cm the height of the centroid of the vorticity grows faster than do both the height of maximum velocity in the base flow and the thickness of the boundary-layer base flow. This result indicates that the vortices are lifted from the plate by the self-induction effects of the vortex pairs.

5.2. *Growth of the circulation in the vortices*

The PIV velocity measurements also allowed for the acquisition of spatial vortex growth rates. For these experiments, the vortices were forced by placing 2 mm wide $\times$ 10 mm long strips of masking tape on the plate, spaced so as to impose the desired vortex wavelength. These perturbations were necessary to obtain uniform growth rates for the vortices, and made it possible to vary the wavelength of the vortices while keeping all other conditions constant. This method of perturbing the flow was used by Klebanoff, Tidstrom & Sargent (1961) in their study of boundary-layer stability.

Two different methods of finding growth rates were developed. First, an attempt was

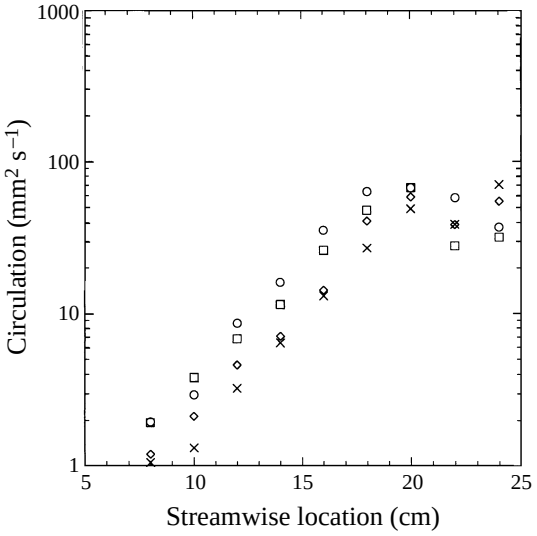

FIGURE 12. Growth of circulation and saturation at 16–20 cm. Each symbol represents a different vortex.

made to find vortex growth rates from the plan-view velocity measurements. However, this method was rejected because refraction of the laser sheet close to the plate by the temperature gradient caused the sheet to be bent. Furthermore, a laser sheet cannot cut through similar locations in the vortices at all streamwise locations because the thickness of the boundary layer increases nonlinearly with distance from the leading edge. Instead, the cross-section (y, z-plane) velocity fields were found to be more useful for measuring growth rates. In order to determine the growth of the vortices, the laser sheet was traversed in the streamwise direction and images acquired at successive downstream locations. From these images, the circulation in the vortices was calculated at each station by integrating the vorticity field over the area of each vortex. Each complete run consisted of images from eight to 10 streamwise stations with approximately 6 s between stations. It is noted here that for a 1 cm thick laser sheet, the spatial resolution is somewhat reduced. If the growth rate is sufficiently large, the decreased spatial resolution caused by the thick light sheet will have some effect on the growth measurements. One can view this effect as spatially averaging the circulation measurements in the streamwise direction over the sheet thickness. Averaging this way will only produce an error if the growth curve deviates significantly from linear over the 1 cm distance. This turns out not to be the case, as discussed in §5.2.1.

Circulation growth data obtained from an early experiment with $\theta = 30$ degrees, $\Delta T = 10\ ^{\circ}C$, and $Pr = 5.8$ are shown in figure 12. The data from four different vortices are shown up to $x = 24$ cm just prior to the onset of wavy motion in some of the vortices. It is seen that the circulation, after an initial nearly exponential growth, becomes saturated between 16 and 20 cm. The point of saturation does not occur at the same streamwise location for all vortices, and the magnitude of the circulation at each streamwise location varies between vortices. These variations are not unexpected, as the height and width of the vortices as well as the critical transition points were observed to vary between vortices. This is in agreement with the observations of previous experiments, such as those by Sparrow & Husar (1969), Lloyd & Sparrow (1970), and Cheng & Kim (1988). In all subsequent circulation growth experiments, data were collected up to the region of saturation.

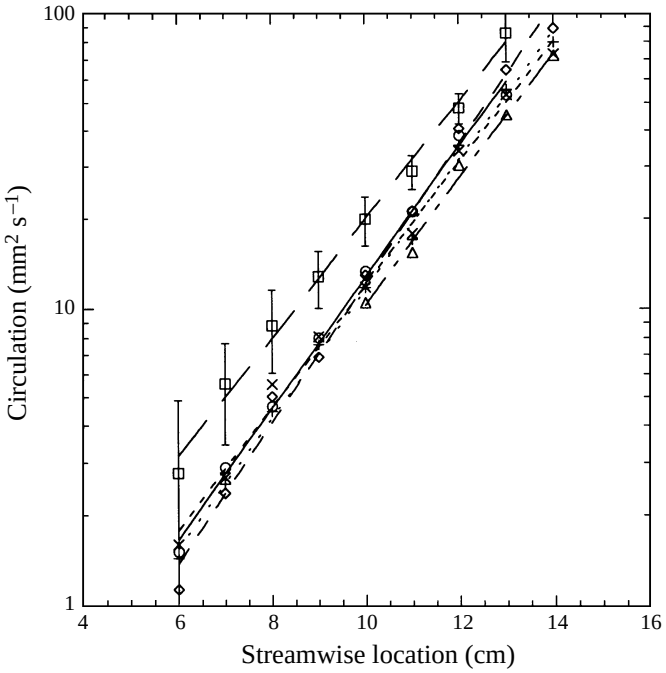

FIGURE 13. Typical results of circulation growth in the streamwise direction. Each type of symbol represents a different vortex, and lines of equation (5.1) are fitted to each vortex.

Figure 13 shows a typical graph of the growth of circulation with streamwise distance for a single experimental run plotted on a semilog scale. The conditions for this plot are $Pr = 5.8$, $\theta = 40$ degrees, and $\Delta T = 10\,^{\circ}\mathrm{C}$. Each symbol in this figure represents a different vortex, and the error bars are estimates of the uncertainty in the circulation values from one set of experimental measurements and are deemed typical for all measurements. No horizontal error bars are needed since the extent of the symbols indicates the uncertainty in x, ± 1 mm. The fact that the data fall on straight lines indicates that the circulation, Γ, grows exponentially, having the form:

$$\Gamma = A \exp(Bx). \tag{5.1}$$

Lines of exponential growth were least-square fitted to the data. Three runs up the plate, such as the one used to construct figure 13, were completed during each experiment, and the number of vortices averaged for each growth rate varied from 45 to 60.

5.2.1. *Effect of streamwise location of tape perturbations on growth rates*

Growth rates were determined for several different conditions. First, the streamwise location of the tape perturbations was varied. Figure 14 shows the results when the tape strips are set at 2, 3 and 5 cm from the start of the heated region of the plate for $Pr = 5.8$, $\theta = 30$ degrees, and $\Delta T = 10\,^{\circ}\mathrm{C}$. Here, only lines of exponential growth (equation (5.1)) fitted to each set of data are shown. Note that while the distance at which the vortices are forced varies by 3 cm, the growth occurs at nearly identical streamwise locations. This indicates that the streamwise locations of the tape perturbations are not critical when placed in the range tested. The initial amplitude, A, and growth coefficient, B, vary slightly, but are well within the typical amount of scatter observed between experiments at identical conditions. Based on these results,

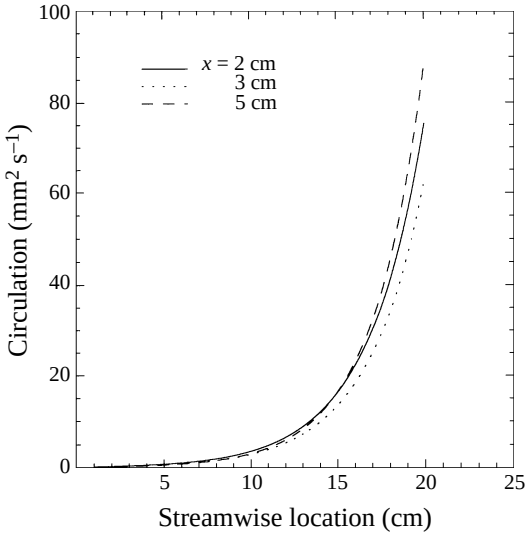

FIGURE 14. The effect of the locations of the perturbations on circulation growth. The tape perturbations are set at 2, 3 and 5 cm from the leading edge.

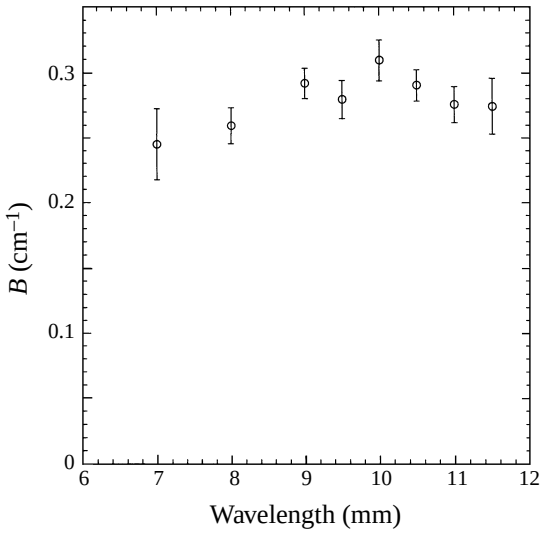

FIGURE 15. Growth coefficient *vs.* spanwise wavelength. The flow conditions are: $\theta = 30$ degrees, $Pr = 5.8$, and $\Delta T = 10$ °C.

the tape strips were set at 3 cm from the start of the heated region of the plate for all experiments at $\theta = 30$ degrees and $\theta = 40$ degrees. The tape strips were moved upstream to the start of the heated region of the plate for experiments at $6 = 50$ degrees and $\theta = 60$ degrees to avoid tripping the vortices near the location at which they begin growing naturally.

5.2.2. *Effect of wavelength on growth rates*

Next, the wavelength of the vortices was varied. It was anticipated that the maximum growth rate would be measured when the vortices were forced at the most unstable wavelength. Figure 15 shows the growth coefficient B from equation (5.1)

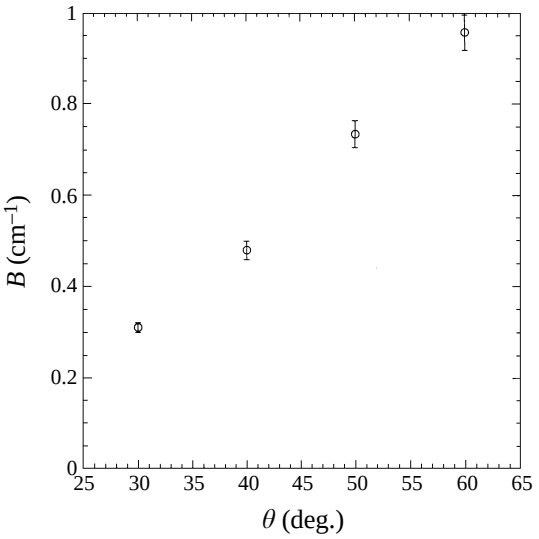

FIGURE 16. Growth coefficient *vs.* θ. The flow conditions are: $Pr = 5.8$, $\Delta T = 10$ °C, and input wavelength = 10 mm.

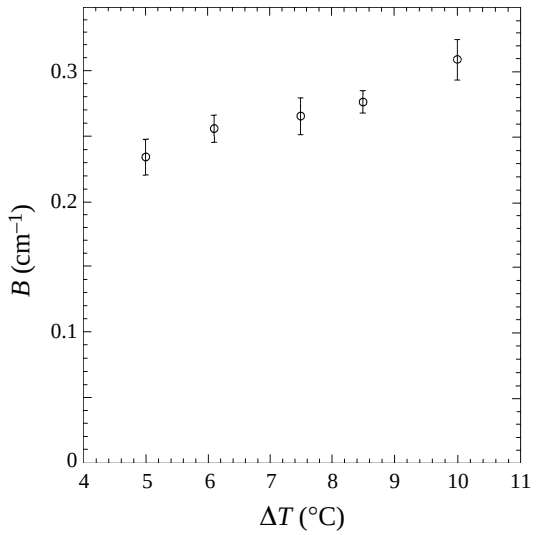

FIGURE 17. Growth coefficient *vs.* ΔT. The flow conditions are: $\theta = 30$ degrees, $Pr = 5.8$, and input wavelength = 10 mm.

plotted versus wavelength. All growth rates were determined with the plate at $\theta = 30$ degrees, $Pr = 5.8$, and $\Delta T = 10$ °C. The wavelengths were varied from 7 to 11.5 cm by varying the spacing of the tape strips used to trip the vortices. The error bars show a 95% confidence level. The data show a shallow peak, with the highest value of 0.31 cm^{-1} at a wavelength of 10 mm. This is approximately the wavelength observed for the unforced instability at these conditions with the Schlieren system. When a wavelength larger than 11.5 mm was forced, the vortices tended to occur at a wavelength shorter than that of the perturbations. At the shortest wavelength tested (7 mm), some vortices did not grow at all, i.e. they had an identical circulation at each downstream location until the flow became unsteady. The wavelength of the vortices

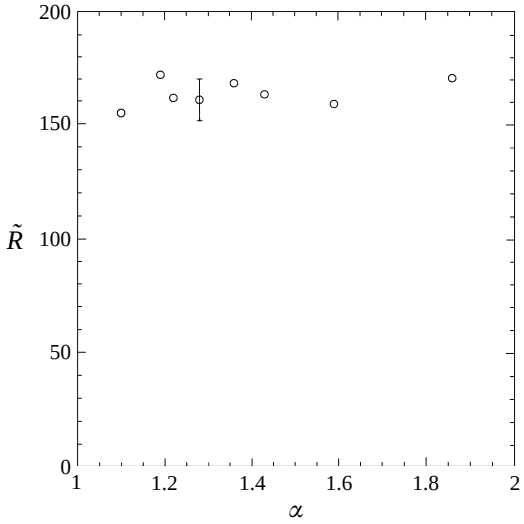

FIGURE 18. $\tilde{R}_c$ *vs.* wavenumber.

at the location at which the vortices stopped growing was usually approximately 1 mm greater than the wavelength at which the vortices were forced. This was consistent whether the forced wavelength was less than or greater than the most unstable wavelength, which is notable because one might expect the wavelength of the vortices to tend toward the most unstable wavelength.

5.2.3. *Effect of θ and ΔT on growth rates*

The effect of the angle of inclination of the plate on growth rates was also studied. These results are shown in figure 16, where $Pr = 5.8$, $\Delta T = 10\,^{\circ}\mathrm{C}$, and input wavelength = 10 mm. Note that the growth rate increases with increasing θ, as does the scatter in the data, which is evident from the error bars on the plot. The increase in the scatter with angle of inclination probably occurs because the distance over which the growth of the vortices takes place decreases as the angle of inclination increases and errors in the circulation calculations are magnified. Also, errors in the positioning of the laser sheet in the flow become more important and, as the laser sheet is 1 cm thick, exact positioning is difficult.

The temperature difference between the plate and ambient was also varied. Figure 17 shows the results, where $\theta = 30$ degrees, $Pr = 5.8$, and input wavelength = 10 mm. As might be expected, the growth rates increase with increasing temperature difference.

5.2.4. *$\tilde{R}_c$ defined using growth curves*

The growth curves can be used to define critical values for the onset of vortices. The location of the onset of vortices was chosen to be the streamwise location at which the value of the circulation is $10\ \mathrm{mm^2\,s^{-1}}$. This value was chosen because, for values of circulation of the order $1\ \mathrm{mm\,s^{-1}}$, the noise in the data is the same order of magnitude as the circulation, while at $10\ \mathrm{mm^2\,s^{-1}}$ this noise is no longer significant. In addition, $10\ \mathrm{mm^2\,s^{-1}}$ is approximately 10% of the maximum circulation the vortices usually achieve. In the sample growth data shown in figure 13, this point occurs approximately 9 cm from the start of the heated region of the plate for most of the vortices. This threshold is somewhat arbitrary, and a lower one would have been chosen if the data had had a lower noise level

The data gathered for various values of $\tilde{R}_c$ and θ were examined to determine $\tilde{R}_c$.

Average values for the curve fit coefficients A and B from equation (5.1) were found at each ΔT and θ, and from these 10 mm^2 s^{-1} threshold was found. The mean $\tilde{R}_c$ determined by this method was 155, with a variation of 12% between the highest and lowest value of $\tilde{R}_c$. Recall that the Schlieren method yielded $\tilde{R}_c = 145$, which corresponds to a circulation threshold of approximately 7.9 mm^2 s^{-1}. The closeness of the values of $\tilde{R}_c$ determined by the growth rates and by the Schlieren system is coincidental, as the threshold for the onset of vortices determined by growth rates is somewhat arbitrary. The stability analysis of Chen *et al.* (1991) predicted $\tilde{R}_c = 24.26$, which corresponds to a circulation threshold in the present experiments of approximately 0.3 mm^2 s^{-1}. However, extrapolation from the growth curves is necessary to locate this threshold, as this circulating value occurs upstream of the location of the tape perturbations on the plate.

It is of interest to compare the circulation value of 10 mm^2 s^{-1} to the circulation in the basic flow. For a natural convection boundary layer along a flat plate, the integral of the vorticity from the plate to the edge of the boundary layer is zero. As a result, the total circulation in the boundary layer is zero. However, if one considers only the positive vorticity generated near the plate, the resulting circulation strength of the basic flow up to $\tilde{R}_c = 155$ is approximately 530 mm^2 s^{-1}. It is seen that the value chosen to denote the onset of longitudinal vortices is approximately 2% of the 'circulation' generated in the basic flow near the plate.

The definition of $\tilde{R}_c$ by the threshold technique described above allowed the creation of a wavenumber-versus-$\tilde{R}_c$ curve such as would be constructed for a stability analysis. Figure 18 shows these results. The lengthscale used to extract the non-dimensional wavenumber from the dimensional wavelength was the distance to the onset of the vortices determined by the thresholding method described above. The results are not the smooth curve with a clearly defined minimum that is expected from the stability analyses. Instead, the experimental marginal stability curve is essentially flat, so that the experimental technique cannot resolve a peak. The error bar shown for $\tilde{R}_c$ indicates the estimate of the uncertainties in the experimental measurements.

5.2.5. *Growth of circulation with* $\tilde{R}$

The data on the spatial evolution of the strength of the vortices obtained for the various ΔT and θ can be collapsed into a single growth curve by using the scaled distance from the start of the heated region of the plate $\tilde{R}$ rather than the dimensional distance used above. Figure 19 compares the growth of the circulation in the vortices with both the dimensional and scaled distances from the start of the heated region of the plate. Here lines of exponential growth have been fitted to the data. An average growth curve can be calculated from the data in figure 19(*b*) and the circulation, Γ, can be approximated by the function $\Gamma = \tilde{A}\exp(\tilde{B}\tilde{R})$, where $\tilde{\mathrm{A}} = 0.098$ mm^2 s^{-1} and $\tilde{B} = 0.031$ for the data of the present experiments. Using this approximation and the circulation threshold described above, $\tilde{R}_c = 149$.

This growth curve is useful for comparisons with the calculated spatial growth rates of Iyer & Kelley (1974). They performed a spatial linear stability analysis based on the parallel flow assumption to examine the amplification of both travelling wave and longitudinal vortex instabilities from the location of the onset of instability to the experimentally determined location as observed by Lloyd & Sparrow (1970). Growth curves were plotted in their paper for $\theta = 9$, 16, and 35 degrees, with $Pr = 6.7$. Figure 20 compares the growth curves based on data extrapolated from the present experiments with the results of Iyer & Kelly plotted as the logarithm of the amplitude ratio. The growth rates found by Iyer & Kelly are essentially constant over the range

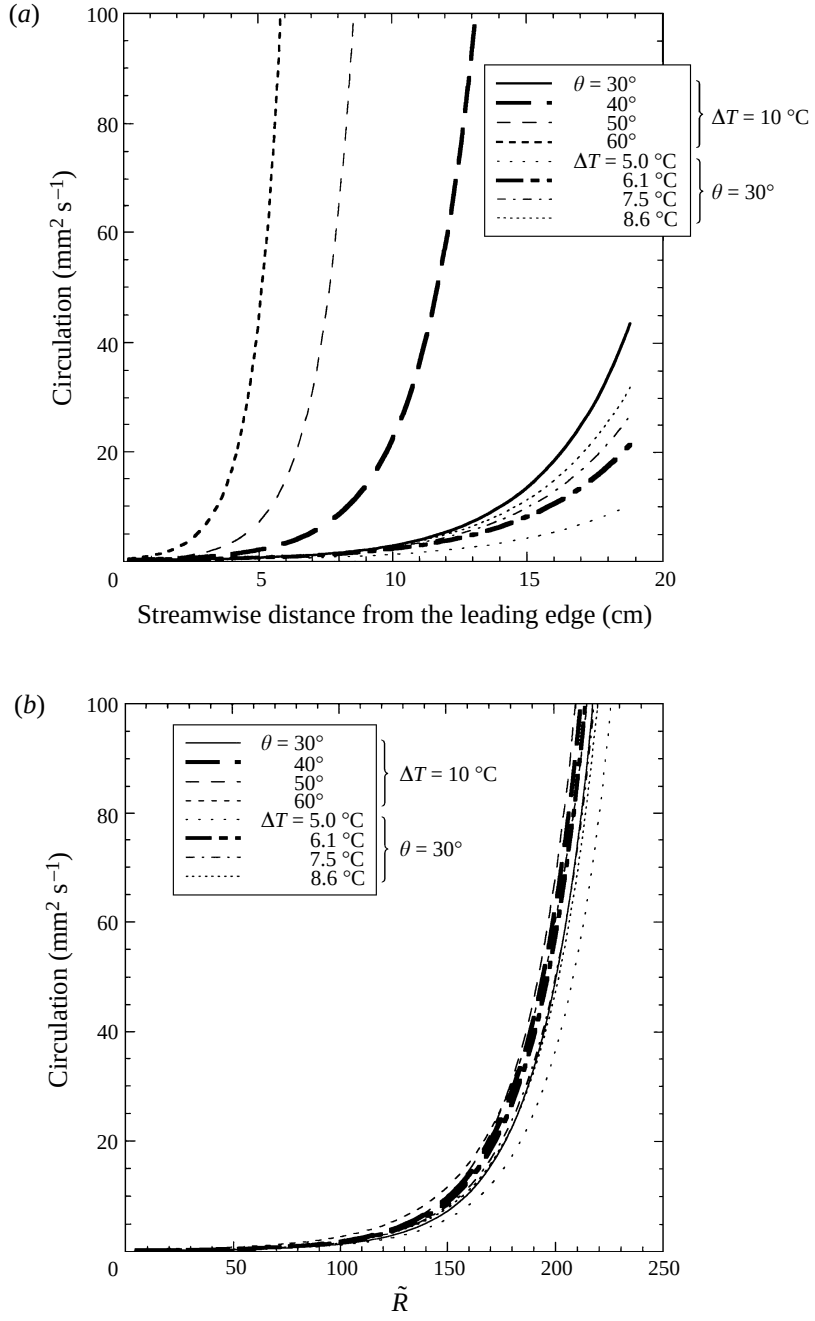

FIGURE 19. Growth of circulation in the vortices with (*a*) dimensional streamwise distance from the start of the heated region of the plate and (*b*) scaled streamwise distance $\tilde{R}$.

of $\tilde{R}$ plotted in figure 20, and the curves for $\theta = 9$ and 16 degrees yield approximate values of $\tilde{B} = 0.039$ and 0.042, respectively; those are 30 % larger than the measured value from the present experiments. Note that Iyer & Kelly express doubts as to the validity of their parallel flow assumption in calculating the growth rate of the vortices at $\theta = 35$ degrees, which can be approximated by $\tilde{B} = 0.051$.

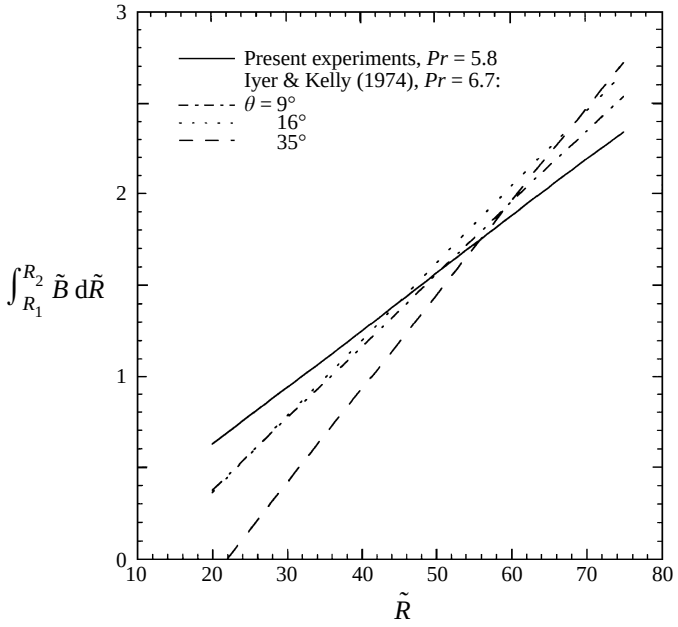

FIGURE 20. Growth curves of present experiments and those of the spatial linear stability analysis of Iyer & Kelly (1974).

6. Conclusions

The following conclusions may be drawn from the results of the present experiments:

(i) The instability characteristics of the boundary-layer flow are very sensitive to the leading-edge condition. PIV measurements indicate that the velocity profile along a vertical heated plate with an unheated starting length agrees well with the similarity solution based on the ideal leading-edge assumption. All results reported in this paper are based on such a leading edge.

(ii) Based on Schlieren data obtained from 32 experiments with the angle of inclination from the vertical varying from 20 to 60 degrees and ΔT from 2 to 23 °C, the onset of longitudinal vortices occurs at $\tilde{R}_c = 145 \pm 5$. $\tilde{R}$ is the modified Reynolds number defined in equation (4.1).

(iii) The pairing and subsequent breakup of the vortices were observed to occur within a short distance of each other along the plate. Thus, these transition points were grouped into one. The data show that the pairing/breakup transition occurs at $\tilde{R}_t = 330 \pm 20$.

(iv) The values of $\tilde{R}_c$ and $\tilde{R}_t$ are quite different from the results of previous experimental investigations and linear stability analyses. The disagreement with the previous experiments may be attributed to the difference in leading-edge conditions and in the sensitivity of the measurement technique. The experimental critical wavenumber is in satisfactory agreement with the results of the linear stability analyses when the experimentally obtained onset distance is used to determine the wavenumber.

(v) Circulation of the vortices determined by the PIV system grows exponentially with the distance from the start of the heated region of the plate. The growth of the circulation in the vortices increases with angle of inclination from the vertical and with ΔT. Also, by defining a suitable circulation threshold, the growth curves can be used to find $\tilde{R}_c = 155$. Finally, growth curves obtained under different conditions can be

collapsed into one when correlated by $\tilde{R}$. Converting the results of Iyer & Kelly (1974) into the $\tilde{R}$ scaling, it was found that their theoretically predicted growth rate is generally higher than the measured value from the present experiments.

Financial support of this research provided by National Science Foundation Grant CTS-9216021 is gratefully acknowledged. We also wish to thank Richard James for his part in the development of the PIV code.

REFERENCES

Adrian, R. J. 1991 Imaging techniques for experimental fluid mechanics. *Ann. Rev. Fluid Mech.* **23**, 261–304.

Chen, C. C., Labhabi, A., Chang, H.-C. & Kelly, R. E. 1991 Spanwise pairing of finite-amplitude longitudinal vortex rolls in inclined free-convection boundary layers. *J. Fluid Mech.* **231**, 73–111.

Chen, T. S. & Tzuoo, K. L. 1982 Vortex instability of free convection flow over horizontal and inclined surfaces. *Trans. ASME* C: *J. Heat Transfer* **104**, 637–643.

Cheng, K. C. & Kim, Y. M. 1988 Flow visualization studies on vortex instability of natural convection flow over horizontal and slightly inclined constant-temperature plates. *Trans. ASME* C: *J. Heat Transfer* **110**, 608–615.

Ede, A. J. 1967 Advances in free convection. In *Advances in Heat Transfer* (ed. J. P. Hartnett & T. F. Irvine), vol. 4. Academic.

Gebhart, B., Jaluria, Y., Mahajan, R. L. & Sammakia, B. 1988 *Buoyancy-Induced Flows and Transport*. Hemisphere.

Haaland, S. E. & Sparrow, E. M. 1973 Vortex instability of natural convection flow on inclined surfaces. *Intl J. Heat Mass Transfer* **16**, 2355–2367.

Iyer, P. A. & Kelly, R. E. 1974 The stability of the laminar free convection flow induced by a heated inclined plate. *Intl J. Heat Mass Transfer* **17**, 517–525.

Kierkus, W. T. 1968 An analysis of laminar free convection flow and heat transfer about an inclined isothermal plate. *Intl J. Heat Mass Transfer* **11**, 241–253.

Klebanoff, P. S., Tidstrom, K. D. & Sargent, L. M. 1961 The three-dimensional nature of boundary-layer instability. *J. Fluid Mech.* **12**, 1–34.

Lloyd, J. R. 1974 Vortex wavelength in the transition flow adjacent to upward facing inclined isothermal surfaces. *Proc. 5th Intl Heat Transfer Conf.* **3**, 34–37.

Lloyd, J. R. & Sparrow, E. M. 1970 On the instability of natural convection flow on inclined plates. *J. Fluid Mech.* **42**, 465–470.

Lock, G. S. H., Gort, C. & Pond, G. R. 1967 A study of instability in free convection from an inclined plate. *Appl. Sci. Res.* **18**, 171–182.

Moutsoglou, A., Chen, T. S. & Cheng, K. C. 1981 Vortex instability of a mixed convection flow over a horizontal flat plate. *Trans. ASME* C: *J. Heat Transfer* **103**, 257–261.

Rich, B. R. 1953 An investigation of heat transfer from an inclined flat plate in free convection. *Trans. ASME* **75**, 489.

Shaukatullah, H. & Gebhart, B. 1978 An experimental investigation of natural convection flow on an inclined surface. *Intl J. Heat Mass Transfer* **21**, 1481–1490.

Sparrow, E. M. & Husar, R. B. 1969 Longitudinal vortices in natural convection flow on inclined surfaces. *J. Fluid Mech.* **37**, 251–255.

Tritton, D. J. 1963 Transition to turbulence in the free convection boundary layers on an inclined heated plate. *J. Fluid Mech.* **16**, 417–435.

Vliet, G. C. 1969 Natural convection local heat transfer on constant-heat-flux inclined surfaces. *J. Heat Transfer* **91**, 511.

Willert, C. E. & Gharib, M. 1991 Digital particle image velocimetry. *Exps. Fluids* **10**, 181–193.

Zuercher, E. J. 1996 An experimental investigation of the stability of the natural convection flow on an inclined, heated plate. MS thesis, The University of Arizona.